Molecular Immunology 56 (2013) 693–697

Contents lists available at ScienceDirect

Molecular Immunology

journal homepage: www.elsevier.com/locate/molimm

Short communication

Conformational plasticity at the IgE-binding site of the B-cell receptor CD23

Balvinder Dhaliwal[a,b,*], Marie O.Y. Pang[a,b], Daopeng Yuan[a,b], Norhakim Yahya[a,b], Stella M. Fabiane[a,b], James M. McDonnell[a,b], Hannah J. Gould[a,b], Andrew J. Beavil[a,b], Brian J. Sutton[a,b,**]

[a] King's College London, Randall Division of Cell and Molecular Biophysics, New Hunt's House, Guy's Campus, London SE1 1UL, UK
[b] MRC & Asthma UK Centre in Allergic Mechanisms of Asthma, London, UK

ARTICLE INFO

Article history:
Received 1 July 2013
Accepted 8 July 2013
Available online 7 August 2013

Keywords:
Allergy
Immunoglobulin E
Antibody–receptor interactions
Immunology
X-ray crystallography

ABSTRACT

IgE antibodies play a central role in allergic disease. They recognize allergens *via* their Fab regions, whilst their effector functions are controlled through interactions of the Fc region with two principal cell surface receptors, FcεRI and CD23. Crosslinking of FcεRI-bound IgE on mast cells and basophils by allergen initiates an immediate inflammatory response, while the interaction of IgE with CD23 on B-cells regulates IgE production. We have determined the structures of the C-type lectin "head" domain of CD23 from seven crystal forms. The thirty-five independent structures reveal extensive conformational plasticity in two loops that are critical for IgE binding.

1. Introduction

Immunoglobulin E (IgE) antibodies play a central role in allergic disease. They recognize allergens through their Fab regions, and interact with two principal cell surface receptors, FcεRI and CD23, *via* their Fc regions (Gould and Sutton, 2008). FcεRI, found mainly on mast cells and basophils, binds IgE with high affinity ($K_A = 10^{10}$–10^{11} M^{-1}) and is primarily responsible for allergic sensitization and the inflammatory response in which minute amounts of allergen crosslink FcεRI-bound IgE, triggering cell degranulation. In contrast, IgE binding to CD23 (also known as FcεRII) is central to the mechanism regulating IgE synthesis (Gould and Sutton, 2008). CD23, expressed on B-cells, is unique amongst Ig receptors as it belongs to the C-type lectin-like domain superfamily (Zelensky and Gready, 2005). It consists of three C-type lectin 'head' domains connected to the cell membrane *via* a trimeric α-helical coiled–coiled 'stalk'. A single head domain binds to IgE-Fc with an affinity of $K_A \sim 10^6$ M^{-1} (Shi et al., 1997), although the avidity of the trimer substantially enhances the interaction (McCloskey et al., 2007). The stalk region of CD23 is susceptible to attack by various proteases to yield soluble trimeric (for instance, after site-specific cleavage with ADAM10 (Weskamp et al., 2006)) as well as monomeric forms of CD23. Along with the membrane-bound form, soluble CD23 has been implicated in both positive and negative regulation of IgE synthesis (Gould and Sutton, 2008). When expressed on gastrointestinal cells, CD23 is also involved in the transport of IgE-allergen complexes across the gut epithelial barrier, thus contributing to food allergenic reactions (Tu et al., 2005). Similarly, CD23 expressed on respiratory tract epithelial cells promotes airway allergic

Abbreviations: IgE, immunoglobulin E; ADAM10, a disintegrin and metalloproteinase domain-containing protein 10; NOE, nuclear Overhauser effect; PDB, Protein Data Bank.

* Corresponding author at: King's College London, Randall Division of Cell and Molecular Biophysics, New Hunt's House, Guy's Campus, London SE1 1UL, UK. Tel.: +44 020 7848 6422; fax: +44 020 7848 6435.
** Corresponding author at: King's College London, Randall Division of Cell and Molecular Biophysics, New Hunt's House, Guy's Campus, London SE1 1UL, UK. Tel.: +44 020 7848 6423; fax: +44 020 7848 6410.
E-mail addresses: bal.dhaliwal@kcl.ac.uk (B. Dhaliwal), brian.sutton@kcl.ac.uk (B.J. Sutton).

0161-5890
http://dx.doi.org/10.1016/j.molimm.2013.07.005

inflammation (Palaniyandi et al., 2011). An understanding of the CD23-IgE interaction therefore has many implications for the prevention of allergic disease.

2. Materials and methods

2.1. Protein purification

Recombinant human derCD23 (Ser156–Glu298) was expressed, refolded and purified as previously described (Dhaliwal et al., 2012; Hibbert et al., 2005).

2.2. Crystallization and data collection

During trials to crystallize various complexes of derCD23, six novel crystal forms of derCD23 alone were identified. Subsequent crystal optimizations used only derCD23.

All crystals were obtained by the hanging drop vapor diffusion method at 291 K and grew to their maximal size between four days and two weeks.

Prior to crystallization, derCD23 was concentrated and buffer-exchanged into 25 mM Tris–HCl pH 7.5, 125 mM NaCl and 0.05% sodium azide. Crystals were obtained by mixing derCD23 with an equal volume of reservoir solution. Crystal forms A, B and C were grown by mixing 3.5 mg/ml derCD23 with 16% (w/v) PEG 6000, 2% (v/v) 1,6-hexanediol, 0.05 M ammonium sulfate and 0.1 M sodium acetate pH 4.7 (Yuan et al., 2013); 18% (w/v) PEG 6000, 2% (v/v) 1,6-hexanediol, 0.05 M ammonium sulfate and 0.1 M sodium acetate pH 4.5; and 25% (w/v) PEG 4000, 0.15 M ammonium sulfate and 0.1 M MES pH 5.5, respectively. Crystal form D was grown by mixing 5 mg/ml derCD23 with 22.5% (w/v) PEG 3350, 0.2 M ammonium sulfate and 0.1 M MES pH 5.5. Crystal form E grew by mixing 3.8 mg/ml derCD23 and 4 mM $CaCl_2$ with 30% (w/v) PEG 1500 and 0.1 M Malic acid: MES: Tris (MMT) buffer pH 4.25. Crystal form F was obtaining by mixing 4.4 mg/ml derCD23 with 22.5% (w/v) PEG 4000 and 0.1 M sodium citrate pH 4.75. Crystal form G were grown by mixing 2.2 mg/ml derCD23 with 3.7 M NaCl and 0.1 M citric acid pH 4.5.

The derCD23 crystals were cryoprotected and then flash-cooled in liquid nitrogen: crystals belonging to forms A, B, C, D and F were cryoprotected by soaking in reservoir solution containing an additional 20% (v/v) glycerol. No additional solution was required to cryoprotect crystals in form E. Crystals belonging to form G were cryoprotected by soaking in 100% (v/v) tacsimate (Hampton Research) pH 5.0.

Diffraction data were collected at 100 K at Diamond Light Source synchrotron beamlines I02, I03, I04 and I24.

2.3. Structure determination

Indexing, integration, and merging of data were carried out with the *HKL2000* (Otwinowski and Minor, 1997), *MOSFLM* (Battye et al., 2011; Powell, 1999) or *XIA2* (Kabsch, 2010; Winter, 2010) suite of programs. The derCD23 structures were solved by molecular replacement with *PHASER* (McCoy et al., 2007) using the Ca^{2+}-free derCD23 (PDB 4G96) (Yuan et al., 2013) crystal structures as the search model.

Crystal form A is the same as that of the previously determined wild-type derCD23 crystal structure (Yuan et al., 2013). However, the four disulfide bridges (C160-C288, C163-C174, C191-C282 and C259-C273) that contribute to the tertiary structure are all intact; in the previous Ca^{2+}-free crystal structure some of the cystine groups underwent radiation damage during X-ray data collection, leading to breakage of some of the disulfide bonds.

Due to the high degree of non-crystallographic symmetry (NCS) in crystal forms B, C and D, reflections were selected for the R_{free} set in thin resolution shells (Fabiola et al., 2006) in the corresponding datasets. Iterative cycles of refinement using *PHENIX* (Adams et al., 2011), *REFMAC5* (Murshudov et al., 2011) and *BUSTER-TNT* (Smart et al., 2012) alternated with manual model building with *COOT* (Emsley et al., 2010). The model was built into $2F_o - F_c$ composite omit, $2F_o - F_c$ and $F_o - F_c$ electron density maps in order to minimize model bias. Initially during refinement, tight NCS restraints were used. These were gradually relaxed, and local structure similarity restraints (or "local NCS") (Murshudov et al., 2011; Smart et al., 2012) applied. During the final cycles of refinement, NCS restraints were released for the structures from crystal forms A, E, F and G. TLS groups (Painter and Merritt, 2005) were generated using the *TLSMD* Web server (Painter and Merritt, 2006). Data processing and refinement statistics are shown in Table 1. Fig. 1 shows the seven asymmetric units identified.

The software, *Hingefind* (Wriggers and Schulten, 1997), *DynDom* (Hayward and Berendsen, 1998), *Contact* (Winn et al., 2011) and *PISA* (Krissinel and Henrick, 2007) were used for structural analysis. All figures presented were generated using *PyMOL* (Schrödinger, 2011).

3. Results and discussion

Previously, we determined the crystal structure of a complex between the soluble monomeric lectin head domain of CD23 (termed derCD23, as it corresponds to a fragment generated by the house dust mite allergenic protease *Der* p 1 (Schulz et al., 1997)) and a sub-fragment of IgE-Fc consisting of the dimer of Cε3 and Cε4 domains, termed Fcε3-4 (Dhaliwal et al., 2012). The complex shows one CD23 head domain binding to each heavy chain of IgE, explaining the known 2:1 stoichiometry (Dhaliwal et al., 2012; McCloskey et al., 2007; Shi et al., 1997). Furthermore we showed that the binding of FcεRI and CD23 to IgE-Fc are allosterically linked: although the binding sites for the two receptors are distant from each other, conformational changes in Fcε3-4 upon derCD23 binding preclude binding of FcεRI, and *vice versa* (Dhaliwal et al., 2012). Conformational changes in free Fcε3-4 (Wurzburg and Jardetzky, 2009), and upon FcεRI binding to Fcε3-4 (Garman et al., 2000) or IgE-Fc (Holdom et al., 2011), have also been described.

The binding of derCD23 to Fcε3-4 is predominantly hydrophilic, involving four salt bridges with hydrogen bonding, and four additional hydrogen bonds. Arg440 in the Cε3-Cε4 linker region of Fcε3-4 forms two hydrogen bonds with Ser254 in loop 4 of derCD23 (Dhaliwal et al., 2012), but this loop is partially disordered (at residues 256 and 257) in the complex. We have recently shown that calcium binding to CD23 enhances its affinity for IgE by binding to the base of loop 4, inducing a *trans* to *cis* isomerization of Pro250 and concomitant ordering and change in conformation of the loop (Yuan et al., 2013). The re-positioned side-chain of Asp258 forms a salt bridge and two new hydrogen bonds with Arg440 of IgE, and the calcium-dependent movement of loop 4 is coupled with conformational changes in loop 1 (Leu226–Glu231) enabling Asp227 to form a salt bridge and two further hydrogen bonds with Arg440 (Yuan et al., 2013). Both loops thus contribute additionally to IgE binding in the presence of calcium.

In this study, we have determined and compared the structures of derCD23 head domains from six new crystal forms together with a previously identified crystal form (Yuan et al., 2013). These structures provide thirty-five independent views of unbound, Ca^{2+}-free derCD23, allowing a comprehensive examination of the conformational variation in the IgE-binding site of CD23. The derCD23 structures show little difference in secondary structure or packing of the core, with Cα r.m.s. deviations ranging from 0.1 to 1.6 Å (over 120 Cα pairs). However, there is considerable plasticity within the IgE-binding loops 1 and 4 (Fig. 2(a)). In addition to conformations that are intermediate between those observed in earlier Ca^{2+}-free

Table 1
Data collection and refinement statistics.

Crystal form		A	B	C	D	E	F	G
PDB accession code		4J6J	4J6K	4J6L	4J6M	4J6N	4J6P	4J6Q
Data processing statistics								
Beamline[a]		I03	I04	I04	I03	I02	I02	I24
Wavelength (Å)		0.9763	0.9763	0.9763	0.9745	0.9795	0.9795	0.9687
Processing software		*HKL2000*	*MOSFLM*	*HKL2000*	*HKL2000*	*MOSFLM*	*XIA2*	*XIA2*
Space group		*P*1	*P*1	*P*1	*P*1	$P2_12_12$	$P2_12_12_1$	$C222_1$
Unit cell parameters	(Å)	a = 52.69	a = 52.56	a = 52.20	a = 52.29	a = 64.26	a = 62.67	a = 59.10
		b = 56.83	b = 56.13	b = 64.37	b = 65.10	b = 73.07	b = 89.92	b = 73.18
		c = 62.49	c = 108.52	c = 112.28	c = 106.78	c = 57.04	c = 101.24	c = 62.88
	(°)	α = 68.45	α = 79.79	α = 75.29	α = 95.26			
		β = 87.83	β = 84.85	β = 82.37	β = 88.88			
		γ = 73.56	γ = 70.22	γ = 89.99	γ = 89.62			
Number of mols/a.u.		4	8	8	8	2	4	1
Solvent content (%)		54	49	58	58	43	47	44
Resolution range (Å)[b]		50.0–1.90 (1.97–1.90)	106.7–2.30 (2.42–2.30)	50.0–3.15 (3.31–3.15)	50.0–2.48 (2.57–2.48)	50.0–2.85 (3.00–2.85)	45.8–1.90 (2.00–1.90)	37.1–2.54 (2.60–2.54)
Observations		188,390	181,392	87,190	107,069	87,366	633,852	29,020
Unique reflections		48,564	47,094	23,522	47,011	6664	45,855	4740
Average redundancy		3.9 (3.9)	3.9 (3.9)	3.7 (3.5)	2.4 (1.9)	13.1 (14.1)	13.8 (13.9)	6.1 (6.3)
Completeness (%)		96.1 (96.3)	92.3 (93.5)	99.0 (98.4)	94.8 (74.9)	99.9 (99.9)	100.0 (100.0)	99.9 (100.0)
Wilson B factor (Å^2)		30.5	47.6	78.6	47.2	46.7	30.2	25.9
$I/\sigma(I)$		24.7 (2.73)	7.6 (3.00)	4.7 (1.47)	8.7 (2.04)	3.5 (1.90)	10.5 (1.60)	7.7 (2.50)
R_{merge}[c]/$R_{p.i.m.}$[d]		0.055[c] (0.395)	0.042[d] (0.257)	0.240[c] (0.664)	0.099[c] (0.294)	0.187[d] (0.352)	0.065[d] (0.544)	0.095[d] (0.364)
Refinement statistics								
Resolution range (Å)		15.8–1.90	45.4–2.30	49.4–3.15	36.3–2.48	48.3–2.85	27.8–1.90	31.6–2.54
Total no. of reflections		48,510	47,059	23,393	46,992	6640	45,754	4727
No. of working reflections		46,045	44,669	22,200	44,616	5986	43,443	3501
No. of test reflections		2465	2390	1193	2376	654	2311	1226
R_{xpct}[e]		0.190	0.191	0.212	0.208	0.252	0.186	0.169
R_{free}[f]		0.217	0.218	0.253	0.243	0.317	0.214	0.240
No. of atoms		4546	8366	8464	8786	2186	4530	1099
Protein		4335	8219	8460	8529	2186	4255	1064
Others[g]		211	147	4	257	0	275	35
R.m.s. bond-length deviation (Å)		0.010	0.010	0.009	0.010	0.009	0.010	0.007
R.m.s. bond-angle deviation (°)		1.03	1.08	1.14	1.15	1.12	1.11	1.11
Mean B factor (Å^2)		41.0	52.9	55.6	31.7	55.2	39.8	29.7
Main chain		36.8	49.0	52.3	29.0	52.2	36.3	28.7
Side chain		45.0	57.1	58.9	34.7	58.2	42.7	30.9
Others[g]		43.1	43.3	7.0	27.2	-	44.3	26.5
R.m.s. backbone B factor deviation[h]		2.2	2.5	2.4	2.3	2.5	2.2	2.4
Ramachandran statistics (%)[i]								
Favored		94.8	95.6	93.2	94.3	85.9	94.4	95.4
Allowed		99.8	100	100	99.6	99.6	99.6	100
Outliers		0.2	0	0	0.4	0.4	0.4	0

[a] Diamond Light Source.
[b] Values in parentheses are for the outer resolution shell.
[c] $R_{merge} = \Sigma|I_{obs} - \langle I\rangle|/\Sigma\langle I\rangle$
[d] $R_{p.i.m.}$ (Precision-indicating merging R factor) = $\Sigma_{hkl}[1/(N-1)]^{1/2}\ \Sigma_i|I_i(hkl) - I(-h-k-l)|/\Sigma_{hkl}\Sigma_i I_i(hkl)$ (Weiss, 2001).
[e] $R_{xpct} = \Sigma_{hkl}||F_{obs}| - |F_{xpct}||/\Sigma_{hkl}\ |F_{obs}|$, where $|F_{obs}|$ and $|F_{xpct}|$ are the observed structure factor amplitude and the expectation of the model structure factor amplitude, respectively (Blanc et al., 2004).
[f] R_{free} equals the R_{xpct} of test set (5% of the data removed prior to refinement).
[g] Water molecules and SO_4^{2-} ions.
[h] R.m.s. deviation between B factors for bonded main-chain atoms.
[i] As defined by MolProbity (Chen et al., 2010).

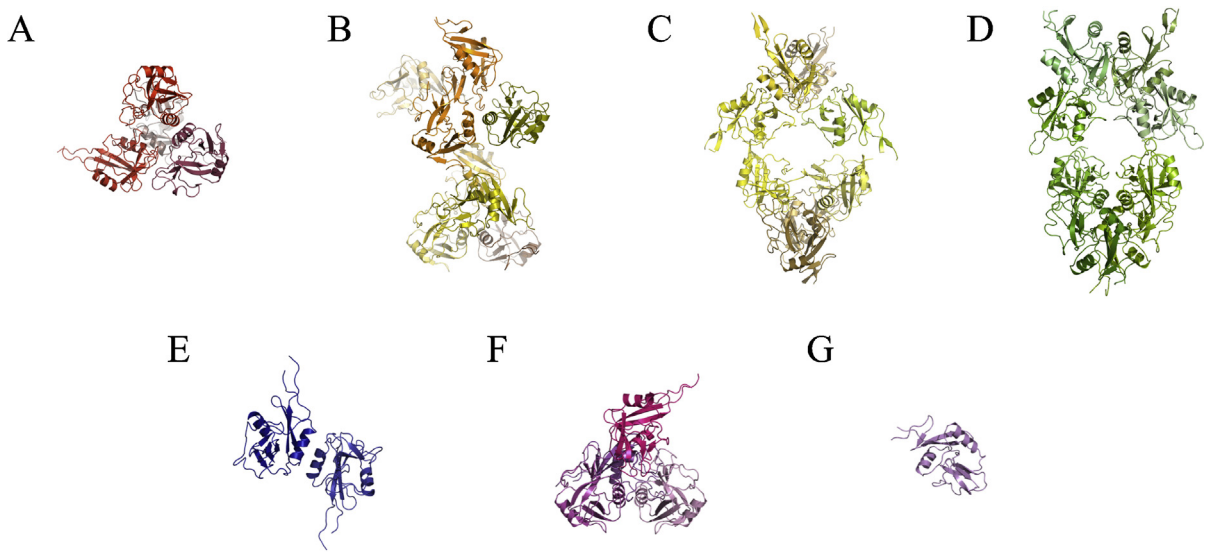

Fig. 1. Asymmetric units of the seven crystal forms of derCD23. The crystal forms A–G are colored red, orange, yellow, green, indigo, blue and violet, respectively, with each molecule in a different shade.

and Ca^{2+}-bound derCD23 (Yuan et al., 2013), loops 1 and 4 are also found to adopt more 'extreme' conformations, lying closer together (*e.g.* molecule D in crystal form F) or further apart (*e.g.* molecule A in crystal form G) than had been seen in any of the earlier structures. In an NMR analysis of derCD23 in solution, residues 253–257 of loop 4 could not be assigned, indicative of mobility on the ms to μs timescale (Hibbert et al., 2005).

Remarkably, all thirty-five of the derCD23 structures can be modeled onto the derCD23-Fcε3-4 crystal structure without any clashes with the antibody, suggesting that all conformations that the head domain of CD23 may adopt free in solution are capable of interacting directly with IgE. Not all thirty-five conformations would make the same number of initial contacts with IgE of course, but upon binding, loops 1 and 4 adopt a single conformation, with

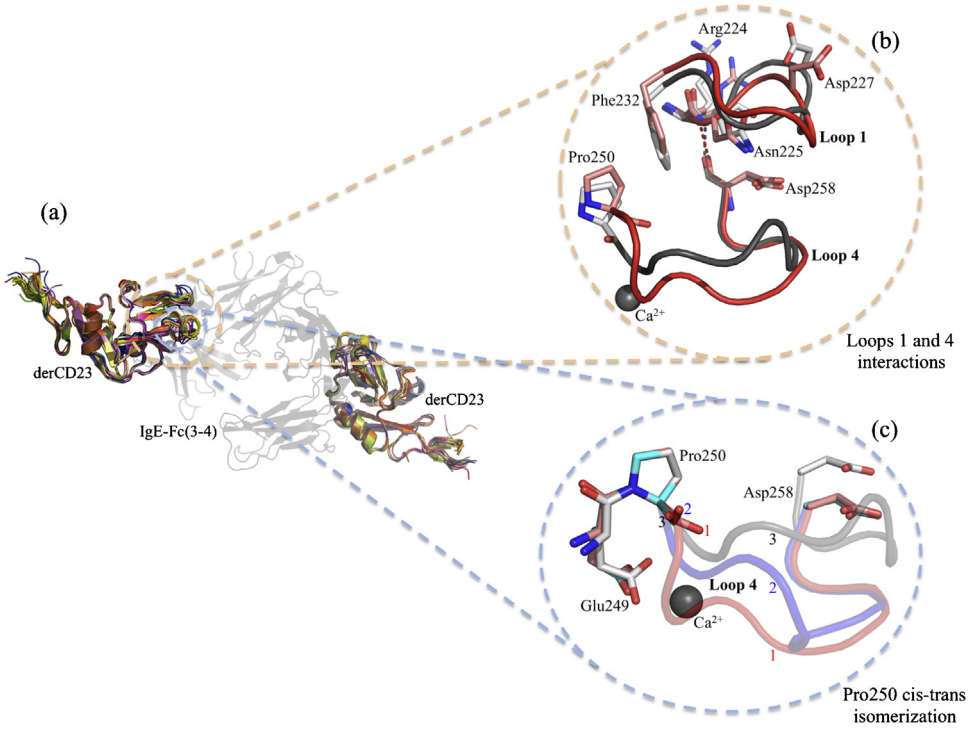

Fig. 2. Conformational plasticity in the B-cell receptor CD23 at loops 1 and 4 of the IgE-binding site. (a) Superimposition of the array of derCD23 molecules onto the derCD23-Fcε3-4 complex (PDB 4EZM) (Dhaliwal et al., 2012). The crystal forms A–G are colored red, orange, yellow, green, indigo, blue and violet, respectively, with each molecule in a different shade. The Fcε3-4 dimer is colored light black. (b) Enlarged view of loops 1 and 4. For clarity, only loops from molecule D crystal form A (red) and molecule A from Ca^{2+}-bound derCD23 (gray, PDB ID 4G9A) are shown. Residues that have been identified as loop 'hinge' points (Wriggers and Schulten, 1997) (Arg224/Asn225 and Phe232 for loop 1, and Pro250 and Asp258 for loop 4) and Asp227 (an IgE interacting residue) are depicted. Also shown is a hydrogen bond between the two loops that is common to all derCD23 structures. (c) Loop 4 from three derCD23 structures superimposed on the atoms of Pro250. The loops depicted are the same as those in (b), along with an "intermediary" loop, molecule E from crystal form B (blue). The Pro250 residues from the Ca^{2+}-bound and intermediary (Ca^{2+}-free) structures (numbered 3 and 2 respectively) are in a *cis*-configuration, while the other Pro250 adopts a *trans*-configuration (numbered 1).

the exception of residues 256 and 257 of loop 4 which remain disordered (Dhaliwal et al., 2012). Only in the presence of Ca^{2+} is loop 4 stabilized in its entirety (Yuan et al., 2013).

Further analysis of the array of derCD23 structures revealed the mechanism by which the movements of loops 1 and 4 are coupled (Fig. 2(b)): they are linked *via* at least one hydrogen bond, namely Asn225–Asp258 in all structures, and a number of van der Waals interactions that ranges from nine (in molecule E of crystal form B, with a partially disordered loop 1) to fifty-two (in molecule D of crystal form F). Moreover, twenty of the thirty-five structures have *cis* configurations for Pro250, while the remainder are *trans* (Fig. 2(c)), implying that in solution the peptide bond is equally likely to be *cis* or *trans* in the absence of calcium; it becomes "locked" as *cis* only upon Ca^{2+} binding (Yuan et al., 2013).

Taken together with the knowledge that the Fcε3-4 region of IgE-Fc exhibits inter-domain flexibility (Wurzburg and Jardetzky, 2009), the extreme loop flexibility in the IgE-binding site of CD23 revealed here presents a picture of two dynamic binding partners. This interaction has potential as a drug target for modulation of IgE production (Rosenwasser and Meng, 2005), and although dynamic targets present difficulties for conventional structure-based inhibitor design, they do offer possibilities for allosteric intervention. Stabilization of less favorable binding conformations is thus a promising strategy, guided by the range of CD23 structures presented here.

Acknowledgments

This study was funded by the Wellcome Trust, Asthma UK and the Medical Research Council (UK); it was also supported by the Diamond Light Source, and we wish to thank the staff at beamlines I02, I03, I04 and I24.

References

Adams, P.D., Afonine, P.V., Bunkoczi, G., Chen, V.B., Echols, N., Headd, J.J., Hung, L.W., Jain, S., Kapral, G.J., Grosse Kunstleve, R.W., McCoy, A.J., Moriarty, N.W., Oeffner, R.D., Read, R.J., Richardson, D.C., Richardson, J.S., Terwilliger, T.C., Zwart, P.H., 2011. The Phenix software for automated determination of macromolecular structures. Methods 55, 94–106.

Battye, T.G., Kontogiannis, L., Johnson, O., Powell, H.R., Leslie, A.G., 2011. iMOSFLM: a new graphical interface for diffraction-image processing with MOSFLM. Acta Crystallographica. Section D, Biological Crystallography 67, 271–281.

Blanc, E., Roversi, P., Vonrhein, C., Flensburg, C., Lea, S.M., Bricogne, G., 2004. Refinement of severely incomplete structures with maximum likelihood in BUSTER-TNT. Acta Crystallographica. Section D, Biological Crystallography 60, 2210–2221.

Chen, V.B., Arendall 3rd, W.B., Headd, J.J., Keedy, D.A., Immormino, R.M., Kapral, G.J., Murray, L.W., Richardson, J.S., Richardson, D.C., 2010. MolProbity: all-atom structure validation for macromolecular crystallography. Acta Crystallographica. Section D, Biological Crystallography 66, 12–21.

Dhaliwal, B., Yuan, D., Pang, M.O.Y., Henry, A.J., Cain, K., Oxbrow, A., Fabiane, S.M., Beavil, A.J., McDonnell, J.M., Gould, H.J., Sutton, B.J., 2012. Crystal structure of IgE bound to its B-cell receptor CD23 reveals a mechanism of reciprocal allosteric inhibition with high affinity receptor FcεRI. Proceedings of the National Academy of Sciences of the United States of America 109, 12686–12691.

Emsley, P., Lohkamp, B., Scott, W.G., Cowtan, K., 2010. Features and development of Coot. Acta Crystallographica. Section D, Biological Crystallography 66, 486–501.

Fabiola, F., Korostelev, A., Chapman, M.S., 2006. Bias in cross-validated free R factors: mitigation of the effects of non-crystallographic symmetry. Acta Crystallographica. Section D, Biological Crystallography 62, 227–238.

Garman, S.C., Wurzburg, B.A., Tarchevskaya, S.S., Kinet, J.P., Jardetzky, T.S., 2000. Structure of the Fc fragment of human IgE bound to its high-affinity receptor Fc epsilonRI alpha. Nature 406, 259–266.

Gould, H.J., Sutton, B.J., 2008. IgE in allergy and asthma today. Nature reviews. Immunology 8, 205–217.

Hayward, S., Berendsen, H.J., 1998. Systematic analysis of domain motions in proteins from conformational change: new results on citrate synthase and T4 lysozyme. Proteins 30, 144–154.

Hibbert, R.G., Teriete, P., Grundy, G.J., Beavil, R.L., Reljic, R., Holers, V.M., Hannan, J.P., Sutton, B.J., Gould, H.J., McDonnell, J.M., 2005. The structure of human CD23 and its interactions with IgE and CD21. Journal of Experimental Medicine 202, 751–760.

Holdom, M.D., Davies, A.M., Nettleship, J.E., Bagby, S.C., Dhaliwal, B., Girardi, E., Hunt, J., Gould, H.J., Beavil, A.J., McDonnell, J.M., Owens, R.J., Sutton, B.J., 2011. Conformational changes in IgE contribute to its uniquely slow dissociation rate from receptor FcvarepsilonRI. Nature Structural & Molecular Biology 18, 571–576.

Kabsch, W., 2010. Xds. Acta crystallographica. Section D, Biological Crystallography 66, 125–132.

Krissinel, E., Henrick, K., 2007. Inference of macromolecular assemblies from crystalline state. Journal of Molecular Biology 372, 774–797.

McCloskey, N., Hunt, J., Beavil, R.L., Jutton, M.R., Grundy, G.J., Girardi, E., Fabiane, S.M., Fear, D.J., Conrad, D.H., Sutton, B.J., Gould, H.J., 2007. Soluble CD23 monomers inhibit and oligomers stimulate IGE synthesis in human B cells. Journal of Biological Chemistry 282, 24083–24091.

McCoy, A.J., Grosse-Kunstleve, R.W., Adams, P.D., Winn, M.D., Storoni, L.C., Read, R.J., 2007. Phaser crystallographic software. Journal of Applied Crystallography 40, 658–674.

Murshudov, G.N., Skubak, P., Lebedev, A.A., Pannu, N.S., Steiner, R.A., Nicholls, R.A., Winn, M.D., Long, F., Vagin, A.A., 2011. REFMAC5 for the refinement of macromolecular crystal structures. Acta Crystallographica. Section D, Biological Crystallography 67, 355–367.

Otwinowski, Z., Minor, W., 1997. Processing of X-ray diffraction data collected in oscillation mode. Methods Enzymology 276, 307–326.

Painter, J., Merritt, E.A., 2005. A molecular viewer for the analysis of TLS rigid-body motion in macromolecules. Acta Crystallographica. Section D, Biological Crystallography 61, 465–471.

Painter, J., Merritt, E.A., 2006. Optimal description of a protein structure in terms of multiple groups undergoing TLS motion. Acta Crystallographica. Section D, Biological Crystallography 62, 439–450.

Palaniyandi, S., Tomei, E., Li, Z., Conrad, D.H., Zhu, X., 2011. CD23-dependent transcytosis of IgE and immune complex across the polarized human respiratory epithelial cells. Journal of Immunology 186, 3484–3496.

Powell, H.R., 1999. The Rossmann Fourier autoindexing algorithm in MOSFLM. Acta Crystallographica. Section D, Biological Crystallography 55, 1690–1695.

Rosenwasser, L.J., Meng, J., 2005. Anti-CD23. Clinical Reviews in Allergy & Immunology 29, 61–72.

Schrödinger, L., 2011. The PyMOL Graphics System, Version 1.5.0.

Schulz, O., Sutton, B.J., Beavil, R.L., Shi, J., Sewell, H.F., Gould, H.J., Laing, P., Shakib, F., 1997. Cleavage of the low-affinity receptor for human IgE (CD23) by a mite cysteine protease: nature of the cleaved fragment in relation to the structure and function of CD23. European Journal of Immunology 27, 584–588.

Shi, J., Ghirlando, R., Beavil, R.L., Beavil, A.J., Keown, M.B., Young, R.J., Owens, R.J., Sutton, B.J., Gould, H.J., 1997. Interaction of the low-affinity receptor CD23/Fc epsilonRII lectin domain with the Fc epsilon3-4 fragment of human immunoglobulin E. Biochemistry 36, 2112–2122.

Smart, O.S., Womack, T.O., Flensburg, C., Keller, P., Paciorek, W., Sharff, A., Vonrhein, C., Bricogne, G., 2012. Exploiting structure similarity in refinement: automated NCS and target-structure restraints in BUSTER. Acta Crystallographica. Section D, Biological Crystallography 68, 368–380.

Tu, Y., Salim, S., Bourgeois, J., Di Leo, V., Irvine, E.J., Marshall, J.K., Perdue, M.H., 2005. CD23-mediated IgE transport across human intestinal epithelium: inhibition by blocking sites of translation or binding. Gastroenterology 129, 928–940.

Weiss, M.S., 2001. Global indicators of X-ray data quality. Journal of Applied Crystallography 34, 130–135.

Weskamp, G., Ford, J.W., Sturgill, J., Martin, S., Docherty, A.J., Swendeman, S., Broadway, N., Hartmann, D., Saftig, P., Umland, S., Sehara-Fujisawa, A., Black, R.A., Ludwig, A., Becherer, J.D., Conrad, D.H., Blobel, C.P., 2006. ADAM10 is a principal 'sheddase' of the low-affinity immunoglobulin E receptor CD23. Nature Immunology 7, 1293–1298.

Winn, M.D., Ballard, C.C., Cowtan, K.D., Dodson, E.J., Emsley, P., Evans, P.R., Keegan, R.M., Krissinel, E.B., Leslie, A.G., McCoy, A., McNicholas, S.J., Murshudov, G.N., Pannu, N.S., Potterton, E.A., Powell, H.R., Read, R.J., Vagin, A., Wilson, K.S., 2011. Overview of the CCP4 suite and current developments. Acta Crystallographica. Section D, Biological Crystallography 67, 235–242.

Winter, G., 2010. xia2: an expert system for macromolecular crystallography data reduction. Journal of Applied Crystallography 43, 186–190.

Wriggers, W., Schulten, K., 1997. Protein domain movements: detection of rigid domains and visualization of hinges in comparisons of atomic coordinates. Proteins 29, 1–14.

Wurzburg, B.A., Jardetzky, T.S., 2009. Conformational flexibility in immunoglobulin E-Fc 3-4 revealed in multiple crystal forms. Journal of Molecular Biology 393, 176–190.

Yuan, D., Keeble, A.H., Hibbert, R.G., Fabiane, S., Gould, H.J., McDonnell, J.M., Beavil, A.J., Sutton, B.J., Dhaliwal, B., 2013. Ca^{2+}-dependent structural changes in the B-cell receptor CD23 increase its affinity for human Immunoglobulin E. Journal of Biological Chemistry.

Zelensky, A.N., Gready, J.E., 2005. The C-type lectin-like domain superfamily. FEBS Journal 272, 6179–6217.